Electrostatic nanolithography in polymers using atomic force microscopy

SERGEI F. LYUKSYUTOV*[1], RICHARD A. VAIA*[3], PAVEL B. PARAMONOV[1], SHANE JUHL[3], LYNN WATERHOUSE[3], ROBERT M. RALICH[1], GRIGORI SIGALOV[2] AND EROL SANCAKTAR[2]

[1]Departments of Physics, The University of Akron, Akron, Ohio 44325, USA

[2]Department of Polymer Engineering, The University of Akron, Akron, Ohio 44325, USA

[3]Materials and Manufacturing Directorate, Air Force Research Laboratory, Wright-Patterson Air Force Base, Ohio, USA

*e-mail: sfl@physics.uakron.edu; richard.vaia@wpafb.af.mil

Published online: 22 June 2003; doi:10.1038/nmat926

The past decade has witnessed an explosion of techniques used to pattern polymers on the nano (1–100 nm) and submicrometre (100–1,000 nm) scale, driven by the extensive versatility of polymers for diverse applications, such as molecular electronics[1,2], data storage[3], optoelectronics[4], displays[5], sacrificial templates[6,7] and all forms of sensors. Conceptually, most of the patterning techniques, including microcontact printing (soft lithography)[8], photolithography[9,10], electron-beam lithography[11], block-copolymer templating[12,13] and dip-pen lithography[14], are based on the spatially selective removal or formation/deposition of polymer. Here, we demonstrate an alternative and novel lithography technique—electrostatic nanolithography using atomic force microscopy—that generates features by mass transport of polymer within an initially uniform, planar film without chemical crosslinking, substantial polymer degradation or ablation. The combination of localized softening of attolitres (10^2–10^5 nm^3) of polymer by Joule heating, extremely non-uniform electric field gradients to polarize and manipulate the soften polymer, and single-step process methodology using conventional atomic force microscopy (AFM) equipment, establishes a new paradigm for polymer nanolithography, allowing rapid (of the order of milliseconds) creation of raised (or depressed) features without external heating of a polymer film or AFM tip–film contact.

Only a few polymer-patterning approaches have been demonstrated that create controlled nanoscale structures by mass transport of polymer within an initially uniform, planar film. Numerous applications such as data storage and sensor arrays benefit from the unique characteristics afforded by this patterning approach, including the ability to modify structures after initial formation, elimination of pattern-development processing steps, minimization of associated small-molecule contaminants and access to alternative chemistries and materials. Lithographically induced self-construction in polymer films[15,16] is based on externally driven enhancement of a surface instability at an interface between two dielectrics. When electrostatic and/or van der Waals pressure overcomes Laplace pressure, a film heated above the glass-transition temperature (T_g) becomes highly unstable with regard to small perturbations. The physical description of the dynamical instability of a dielectric liquid in a strong electric field[17] (10^7–10^8 V m^{-1}) has been implemented for polymer melts, and a wide range of architectures with submicrometre features (~100 nm) have been created[18]. The technique is not thoroughly understood though, and feature generation is slow, in some instances requiring hours. Thermomechanical writing[19], is based on the indentation of an AFM tip into a polymer surface, which is softened locally by heat from the AFM tip. Current implementation of this technique by researchers at IBM using a 32×32 array of individually addressed AFM tips (MILLIPEDE)[20,21] has demonstrated data storage densities of 400–500 Gb inch^{-2} in polymethylmethacrylate (PMMA), although AFM-tip–polymer contact and microfabrication of arrays of AFM tips with heating elements are still technological challenges.

AFM-assisted electrostatic lithography (AFMEN) generates features by simply biasing (0–20 V) a highly conductive tungsten carbide K-TEK tip across a thin polymer film (thickness ~20–100 nm, surface roughness 0.5–1 nm) resting on a grounded conductive layer (sputter-deposited Au–Pd film on a silicon wafer). For a wide range of process conditions, raised features (1–50 nm) have been observed. Figure 1 displays representative structures formed by AFMEN in polymers with different physico–chemical properties, demonstrating the generality of the procedure. The nanoscale features were patterned using constant force as well as height AFM (with and without feedback loop enabled, respectively). Dots were formed by pausing for 0.2–5 seconds with constant bias and lines were created at tip velocities from 0.1 μm s^{-1} to 8 μm s^{-1}. Initially, the tip–surface separation was adjusted in contact mode with a tip set-point such that no mechanical deformation of the surface occurred during image scanning. Previous investigations estimate that for these conditions, the initial tip–surface distance is between 1–5 nm, potentially containing a condensed water meniscus when the voltage is applied to the AFM tip[22]. In general, the specific spatial details of the tip–surface contact profile, as well as cantilever motion, with applied bias during writing is not well understood for various types of AFM nanolithography, including AFMEN. Note that the generation of features larger than the initial tip–surface distance has previously been reported for silicon oxidation[23]. Deviations from idealized pyramidal tip geometry and cantilever distortion resulting in asymmetric interaction between surface and sides of the tip, together with the possibility of cantilever retraction, are possible explanations.

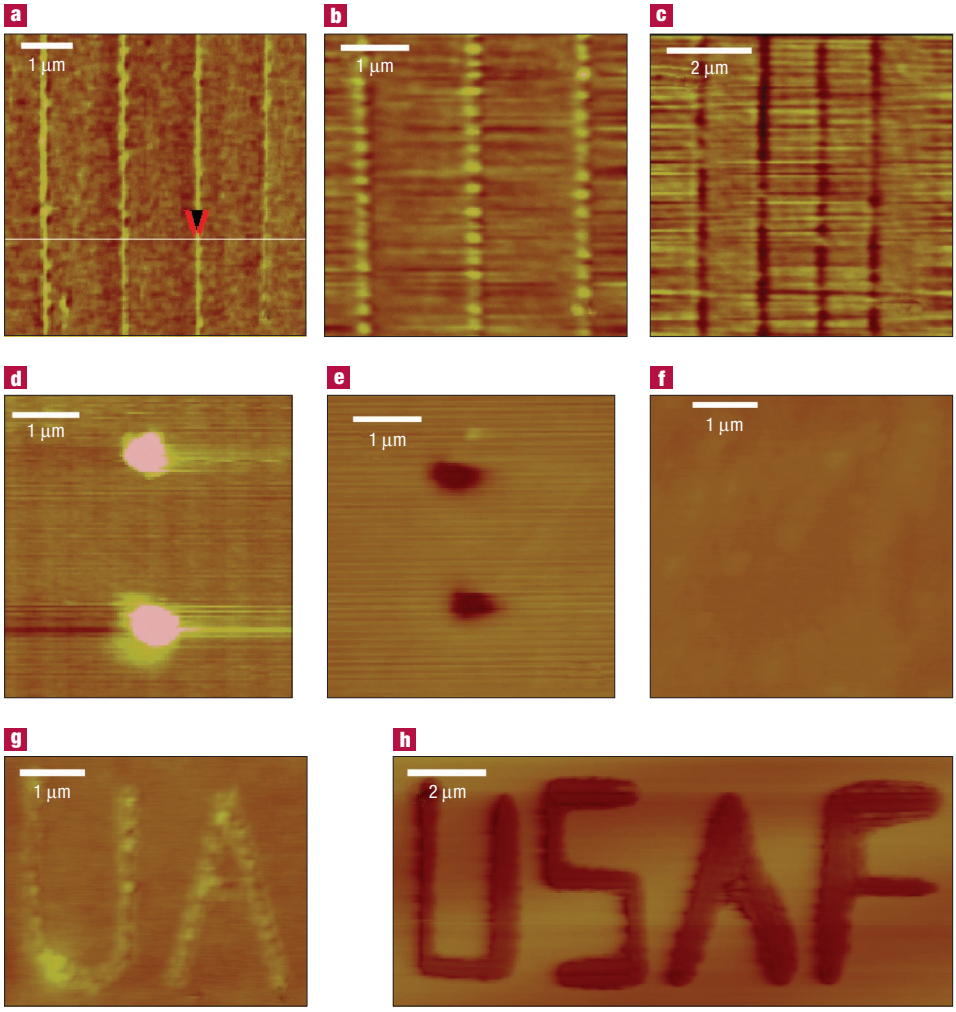

Figure 1 Examples of AFMEN-patterned structures formed in spun-cast, vacuum-annealed polymer films. A Digital Instrument Dimensions 3100 atomic force microscope (AFM) with a Nanoscope IIIa controller and conductive tungsten carbide K-TEK tip was used. Polymers examined included polymethylmethacrylate (PMMA, from Polymer Source; dielectric constant $\varepsilon = 3.2$ (ref. 27); $M_w = 528$k; $M_w/M_n = 1.11$; $T_g = 115$ °C), three molecular weights of polystyrene (PS, from Waters Associates; $\varepsilon = 2.6$ (ref. 24); $M_w = 9.8$k, 110k, 2,300k; $M_w/M_n = 1.03$; $T_g = 87$ °C, 105 °C, 105 °C, respectively), and 12F-polybenzoxazole (12F-PBO ref. 28); $\varepsilon = 2.4$; intrinsic viscosity $\eta = 2.3$ (methane sulphonic acid, 30 °C, 0.12 g per 100 ml); $T_g = 325$ °C). **a–c**, 575k PMMA. **a**, Periodic lines 1 μm pitch, 80 nm wide and 0.32 nm high with an average current of 10 nA (–18 V at 0.1 μm s^{-1}). **b**, Lines with undulating features, 1.65 nm high, with average current of 15 nA (–22 V for 0.1 μm s^{-1}). **c**, Periodic grooves of 1 μm pitch, 460 nm wide and 3.7 nm deep with average current of 50 nA (–25 V at 0.1 μm s^{-1}). **d** and **e**, 12F-PBO. **d**, Dots 500 nm diameter and 6 nm high with instantaneous current of 50 nA (–10 V for 2 s). **e**, Depressions 500 nm diameter and 3 nm deep with instantaneous current of 0.1 μA (–15 V for 2 s). **f–h**, 110k PS. **f**, No features formed with instantaneous current of 2 nA (–6 V for 2 s). **g**, Raised letters 450 nm width and 1.2 nm high with average current of 13 nA (–20 V at 0.1 μm s^{-1}). **h**, Depressed letters 500 nm width and 80 nm deep with average current of 0.1 μA (–30 V at 0.1 μm s^{-1}).

The deviations from an azimuthally symmetric tip–surface junction would lead to the formation of asymmetric structures, which are observed at the upper bias limits of AFMEN.

Three qualitatively distinct regimes—no patterning, raised structures and ablation—can be defined for AFMEN depending on the applied voltage, or alternatively the electrical current. The absolute value of the threshold separating these regions depends on writing conditions, polymer composition and film thickness. As an example, typical structures in 30-nm-thick PMMA films are shown in Fig. 1a–c. Application of input currents less than ~500 pA did not directly create features or latent images that were developable (not shown). As the applied voltage was increased, current abruptly increased (1–10 nA) and raised features were formed (Fig. 1a,b). This is the regime of AFMEN. Feature dimensions increase proportionally to input current. Distorted, asymmetric patterns at the highest currents qualitatively imply that growth may occur askew with respect to the tip apex. Because the polymer is not removed or crosslinked during feature formation, heating the film above T_g without an applied potential, such as with a hot plate, resulted in the removal of the pattern and a featureless surface comparable to the initial film. Finally, for applied voltages generating currents greater than ~0.1 μA, ablation of PMMA resulted, forming holes at the centre of the raised features (Fig. 1c), spreading outward with further current increase.

To provide initial insight into the AFMEM process, consider an idealized approximation of the initial writing geometry as a series of dielectric layers (air, polymer) between a conductive sphere (AFM

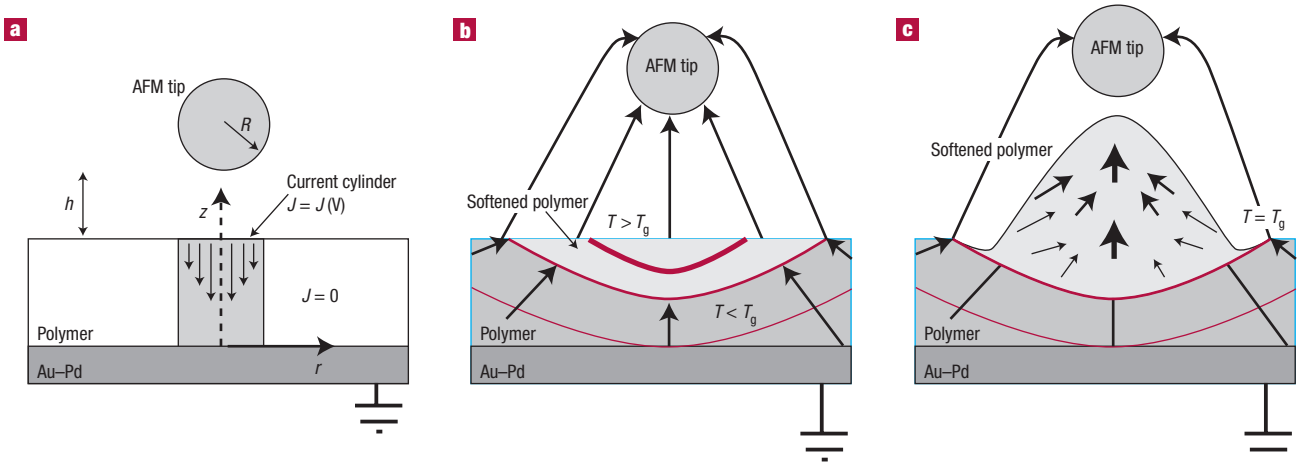

Figure 2 Idealized presentation of the initial writing geometry and feature formation (not to scale). a, Geometrical arrangement of AFM and polymer. Initial tip–surface distance is typically 1–5 nm. In general, the specific spatial details of the tip–surface contact profile, as well as cantilever deformation, with applied bias during writing is not well understood or documented. To a zero-order approximation, the geometrical details arising from the relative orientation of the AFM pyramidal tip with respect to the surface is ignored, and the AFM tip is approximated as a sphere of radius ~35 nm. $J = J(V)$ is the current density, which is a function of the applied (bias) voltage. **b**, Joule heating from amplified current flow increases temperature within the polymer film (isotherms (red solid lines) determined from time-dependent heat-transfer calculations). $T > T_g$ defines the volume of softened viscoelastic polymer. The highly non-uniform electric field (10^9–10^{10} V m^{-1}, estimated by method of images) generates a step electric field gradient (arrows). **c**, The large non-uniform electric field gradient that surrounds the AFM tip produces an electrostatic pressure on the polarizable, softened polymer creating raised features.

tip) and conductive plane (Au–Pd layer), Fig. 2. The geometrical details arising from the relative orientation of the AFM pyramidal tip with respect to the surface is, to a zero order, subsumed into the spherical approximation of the tip. The electric-field distribution inside the polymer film, estimated using the method of images, indicates that for moderate applied voltages (0–20 V) at tip–surface separations of 1–5 nm, an enormously large electric field (10^8–10^{10} V m^{-1}) exists directly under the AFM tip (see Supplementary Information). Additionally, a very steep field gradient occurs in the immediate surrounding polymer where the electrostatic field decreases by a factor of 100–500 within a radius of the idealized AFM tip ($R \approx 35$ nm).

Conductivity σ during AFMEN (estimated from the ohmic character of the I–V response assuming increased current flow I occurs across an area comparable to the AFM tip diameter, ~70 nm) ranged from 10^{-4} to 10^{-2} $(\Omega m)^{-1}$ for PMMA and 5×10^{-4} to 2×10^{-1} $(\Omega m)^{-1}$ for polystyrene (PS). This is substantially greater than the conductivity for these polymers under moderate fields[24] ($\sigma_{PMMA,25\,°C} \sim 10^{14}$ $(\Omega\,m)^{-1}$; $\sigma_{PS,25\,°C} \sim 10^{-18}$ $(\Omega\,m)^{-1}$). The flux of carriers may be generated due to water ionization inside a water meniscus around the AFM tip[22], along with emission of electrons from the tip initiating dielectric breakdown in the polymer film. The extreme electric field estimated within the polymer (Fig. 2) is of the same order of magnitude as the intrinsic dielectric strength of many polymers (10^9 V m^{-1} for PMMA, 6×10^8 V m^{-1} for PS at 20 °C)[24] creating conditions for the electric breakdown through the ultra-thin (20–100 nm) polymer films.

Current flow through the polymer raises the possibility of Joule heating under the AFM tip. Even considering the surrounding as an infinite heat sink, time-dependent heat-transfer calculations indicated that a stable, sustained temperature rise above T_g for a small fraction of the polymer under the AFM tip can be established (see Supplementary Information). This would create a localized region of a dielectric, viscoelastic 'liquid'. Additionally, increased chain dynamics, arising from the density discontinuity at the air–polymer interface, has been shown to decrease the T_g of the polymer in the near-surface region[25], and potentially reducing the necessary temperature increase to create a localized region of molten polymer.

The large non-uniform electric field gradient surrounding the AFM tip will produce an electrostatic pressure, $p(z)$, on this region of localized, polarizable softened polymer ($T > T_g$) of $p(z) = [\{\varepsilon_0(\varepsilon - 1)(\varepsilon + 2)\}/6]E^2(z)$, where z is a cylindrical coordinate defined in Fig. 2a. For representative fields ($E = 1$–6×10^9 V m^{-1}) and polymer dielectric constant ($\varepsilon = 2.5$), pressures of 10–360 MPa are estimated; comparable to the shear modulus of polymer melts. The electrostatic pressure gradient, directed towards the AFM tip, leads to the raised feature formation. Estimating the feature formation process as a steady flow of a non-Newtonian incompressible liquid with a non-slip boundary[26], a 10-nm raised structure would form in 4.26 μs (see Supplementary Information). This is consistent with experimental observations of almost instantaneous feature formation. Furthermore, feature formation should also be easier (faster and lower applied voltages) for polymers of lower molecular weight, which exhibit lower T_g and melt viscosity. This is again consistent with experiment where feature formation was more facile for 9.8k molecular weight polystyrene relative to 110k polystyrene films. Note that feature-formation times are greater than the time required to establish a stable temperature distribution inside the film (see Supplementary Information), indicating that viscosity and polymer mobility should be the limiting factor in feature formation.

An initial quantitative processing relationship can be established by using the experimentally determined current to estimate temperature distributions within the film, and subsequently compare them to the lateral dimensions of the features. Figure 3 compares the estimated diameter of the isotherm at $T = T_g$, and the diameter of raised structures for a relative current increase, I/I_{th}, above the initial threshold for feature formation, I_{th}. The choice of I_{th} provided quantitative agreement with the experimental data, and was within a factor of two of the instantaneous current observed at initial feature formation of dots. Over a narrow current interval, an abrupt increase in feature size corresponds to an increase in the surface area of heated polymer. Further current increase corresponds to a gradual growth in structure size and surface area of the heated polymer. Note that although agreement seems to be excellent, substantially more investigations of the

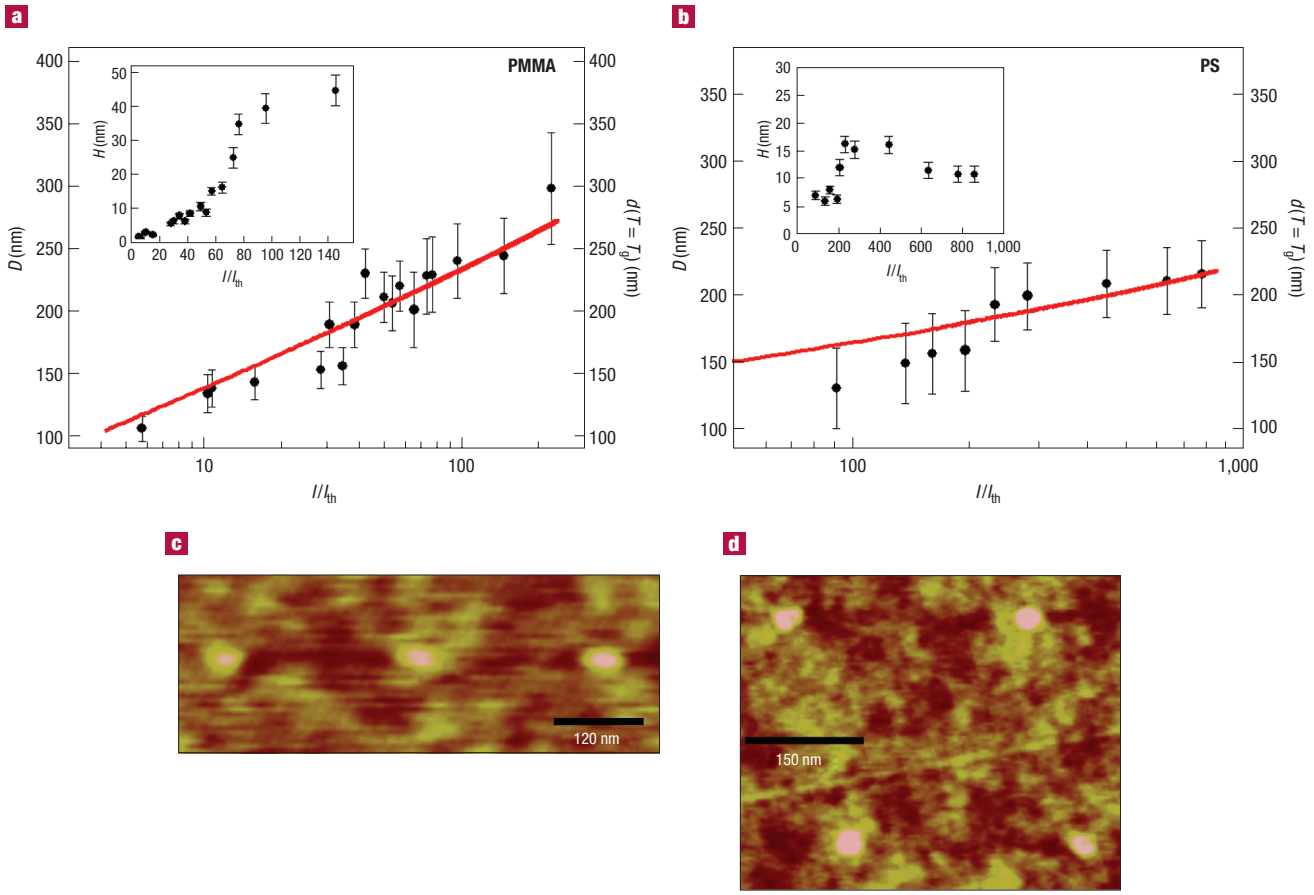

Figure 3 Comparison of the dimensions *D* of AFMEN-produced dots (filled circles) and calculation of the diameter *d* of the isotherm at $T = T_g$ (solid line). Data for *d* obtained through the solution of time-dependent three-dimensional heat equation for **a**, PMMA and **b**, PS. The instantaneous threshold current I_{th} was determined for quantitative agreement: for PMMA, $T_g = 115$ °C, $I_{th} = 8.1$ nA; and for PS, $T_g = 105$ °C, $I_{th} = 4.7$ nA. Parameters used for the solution of the three-dimensional heat equation for PMMA were: conductivity $\sigma = 10^{-4}$–10^{-2} $(\Omega m)^{-1}$, radius $R = 35$ nm, radius of current cylinder ~35 nm, and 0.2 $W(K \times m)^{-1}$; and for PS were $\sigma = 5 \times 10^{-4}$–$2 \times 10^{-1}$ $(\Omega m)^{-1}$, AFM tip radius $R = 35$ nm, current cylinder radius ~ 35 nm, and 0.12 $W(K \times m)^{-1}$. For both polymers, applied voltages were from –15–20 V and dwell times were ~1 s. The current was measured with a Keithley picoammeter between the tip and Au–Pd layer shorted to the grounded stage. **c** and **d**, depict sub-100 nm features in PMMA (50 nm wide, 3 nm height) and PS (23 nm wide, 3 nm height), respectively, using an extrapolation of the processing relationship in **a** and **b**.

perceived trends are necessary because the increase in feature height with current is not yet understood (S. F. Lyuksyutov, R. A. Vaia, P. B. Paramonov and G. Sigalov, manuscript in preparation).

In summary, AFMEN provides a general and conceptually novel approach to nanolithography in polymers using a standard AFM. The basis for feature generation is associated with mass transport of softened polymer liquid in non-uniform electric field. An increase of carrier density, potentially arising from localized dielectric breakdown within the films, creates a 'cylinder' of polymer under the AFM tip susceptible to Joule heating arising from increased current flow. The strong electric field gradient polarizes the viscoelastic polymer, drawing it towards the AFM tip. Material selection and processing that provides a gradual, not catastrophic, dielectric breakdown should provide the optimal polymer film for patterning. The zeroth-order modelling indicates that feature size should depend critically on the thermal characteristics of the polymer, such as T_g, thermal conductivity and temperature dependence of the viscosity. The resolution does not directly depend on the radius of the AFM tip, which is distinctly different from alternative AFM-lithographic techniques. Dielectric properties of the polymer play a secondary role, determining the magnitude of electrostatic pressure but not directly impacting feature width. Through feedback controls for current voltage position and two-dimensional tip arrays, rapid access to both raised and recessed structures should enable ternary (or greater) data storage logic based on relative deflections (positive, zero, negative) from the common plane.

Received 4 February 2003; accepted 22 May 2003; published 22 June 2003.

References

1. Chen, J., Reed, M. A., Rawlett, A. M. & Tour, J. M. Large on-off ratios and negative differential resistance in a molecular electronic device. *Science* **286,** 1550–1552 (1999).
2. Huang, Y., Duan, X., Wei, Q. & Lieber, C. M. Directed assembly of one-dimensional nanostructures into functional networks. *Science* **291,** 630–633 (2001).
3. *The Future of Data Storage Technologies* (International Technology Research Institute World Technology Division Report, Loyola, Maryland, 1999).
4. Lee, K. S. (ed.) *Polymers for Photonic Applications: Nonlinear, Optical and Electroluminescence Polymers* (Springer, New York, 2002).
5. Bastiaansen, C., Tervoort, T. & Weder, C. (eds) *Polymers in Display Applications* (Macromolecular Symposium 154, Wiley, New York, 2000).
6. Wallraff, G. M. & Hinsberg, W. D. Lithographic imaging techniques for the formation of nanoscopic features. *Chem. Rev.* **99,** 1801–1822 (1999).
7. Xia, Y., Rogers, J. A., Paul, K. E. & Whitesides, G. W. Unconventional methods for fabricating and patterning nanostructures. *Chem. Rev.* **99,** 1823–1848 (1999).
8. Xia, Y. & Whitesides, F. M. Soft lithography. *Annu. Rev. Mater. Sci.* **28,** 153–184 (1998).
9. Levinson, H. J. & Arnold, W. H. in *Handbook of Microlithography, Micro Machining and Microfabrciation* Vol.1 (ed. Rai-Choudhury, P.) 11–139 (SPIE, New York, 1997).

10. Bae, Y. *et al.* Tailoring transparency of imageable fluoropolymers at 157 nm by incorporation of hexafluoroisopropyl alcohol to photoresist backbones. *Chem. Mater.* **14,** 1306–1313 (2002).
11. McCord, M. A. & Rocks, M. J. in *Handbook of Microlithography, Micro Machining and Microfabrciation* Vol. 1 (ed. Rai-Choudhury, P.) 139–252 (SPIE, New York, 1997).
12. Park, M., Harrison, C., Chaikin, P. M., Register, R. A. & Adamson, D. H. Block copolymer lithography: periodic arrays of ~10^{11} holes in 1 square centimeter. *Science* **276,** 1401–1404 (1997).
13. Lammertink, R. *et al.* Nanostructured thin films of organic-organometallic block copolymers. One-step lithography with poly(ferrocenylsilanes) by reactive ion etching. *Adv. Mater.* **12,** 98–103 (2000).
14. Piner, R. D., Zhu, J., Xu, F., Hong, S. & Mirkin, C. A. "Dip-Pen" nanolithography. *Science* **283,** 661–663 (1999).
15. Chou, S. Y., Zhuang, L. & Guo, L. Lithographically induced self-construction of polymer microstructures for resistless patterning. *Appl. Phys. Lett.* **75,** 1004–1006 (1999).
16. Chou, S. Y. & Zhuang, L. Lithographically induced self-assembly of periodic polymer micropillar arrays. *J. Vac. Sci. Tech. B* **17,** 3197–3202 (1999).
17. Herminghaus, S. Dynamical instability of thin liquid films between conducting media. *Phys. Rev. Lett.* **83,** 2359–2361 (1999).
18. Schaffer, E., Thurn-Albrecht, T., Russel, T. & Steiner, U. Electrically induced structure formation and pattern transfer. *Nature* **403,** 874–877 (2000).
19. Mamin, H. J. & Rugar, D. Thermomechanical writing with an atomic force microscope tip. *Appl. Phys. Lett.* **61,** 1003–1005 (1992).
20. Vettiger, P. *et al.* The "millipede" – more than one thousand tips for future AFM data storage. *IBM J. Res. Develop.* **44,** 323–340 (2000).
21. Vettiger, P. *et al.* The "millipede" - nanotechnology entering data storage. *IEEE Trans. Nanotech.* **1,** 39–55 (2002).
22. Lyuksyutov, S. F., Paramonov, P. B., Dolog, I. I. & Ralich, R. M. Peculiarities of anomalous electronic current duting AFM-assisted nanolithography on n-type silicon. *Nanotechnology* **14,** 716–721 (2003).
23. Perez-Murano. F., Birkelund. K., Morimoto. K. & Dagata. J. Voltage modulation scanned probe oxidation *Appl. Phys. Lett.* **75,** 199–201 (1999).
24. Kroschwitz, J. I. (ed.) *Electrical and Electronic Properties of Polymers: A State-of-the-Art Compendium* 116–119 (Wiley, New York, 1988).
25. Gorbunov, V. V., Fuchigami, N. & Tsukruk, V. V. Microthermal probing of thin polymer films. *High Perf. Polym.* **12,** 603–610 (2000).
26. Tanner, R. I. *Engineering Rheology* (Clarendon, Oxford, UK, 1985).
27. Osswald, T. A. & Menges, G. *Material Science of Polymers for Engineers* 384–403 (Hansen & Gardner, New York, 1996).
28. Dang, T. D. *et al.* Synthesis and characterization of fluorinated benzoxazole polymers with high T_g and low dielectric constant. *J. Polym. Sci. A* **38,** 1991–2003 (2000).

Acknowledgments

S.F.L. acknowledges support from the US National Research Council, Air Force Office for Scientific Research, and the Air Force Research Laboratory, Materials and Manufacturing Directorate. Correspondence and requests for materials should be addressed to S.F.L. or R.A.V. Supplementary Information accompanies the paper on www.nature.com/naturematerials.

Competing financial interests

The authors declare that they have no competing financial interests.

DISCUSSION OF MODEL CALCULATIONS

ELECTRIC FIELD AND ELECTROSTATIC PRESSURE DISTRIBUTION

The electric field distribution inside the polymer film was computed through the method of images, where the writing geometry was considered as a series of dielectric layers (air, polymer) between a conductive sphere (AFM-tip) and plane (Au-Pd layer). The electric field of a point charge located above a flat dielectric and conductive layer is equivalent to the field of a set of image charges reflected on the air-dielectric and dielectric-conductor interfaces. In turn, each image charge creates a pair of charges of equal magnitude and opposite sign that can be represented by a dipole at the sphere's center along with an infinite set of image dipoles. Since an electric field of a dipole decays more rapidly than that of a point charge, only two image dipoles located in the center of the conductive sphere provide the major contribution to the internal field and thus are the only ones needed to be considered. These calculations verify that a moderate applied voltages (0-20V) at tip-surface separations of 1-5 nm yields enormously large electric fields (10^8-10^{10} V/m) within the polymer film directly under the AFM tip [S1].

A characteristic potential map for a bias voltage $V = -10$ V, tip radius $R = 20$ nm, tip-surface separation $d = 1$ nm, and dielectric constant inside the film $\varepsilon = 2.5$ is shown in Figure S1a. The absolute value of electric field E is plotted for the same system, Figure S1b. The maximum value of the field within the dielectric directly below the idealized AFM tip is found to be $E = 525 \times 10^6$ V m^{-1}.

The equation for electrostatic pressure based on Clausius-Mossotti relation has the following form:

$$p = \frac{\varepsilon_0 E^2}{2} \frac{(\varepsilon - 1)(\varepsilon + 2)}{3} \quad .$$

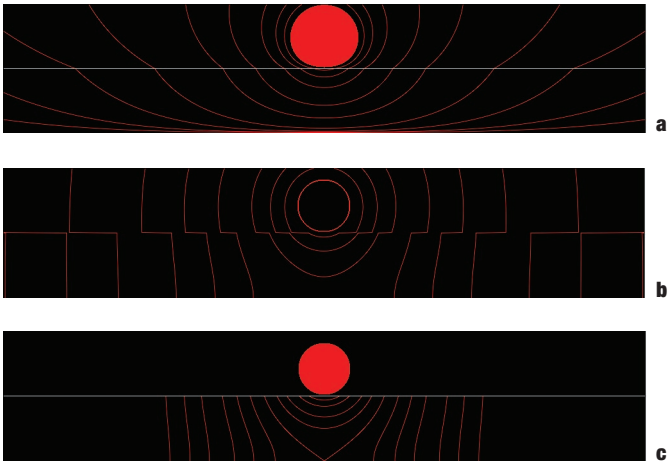

FIGURE S1

Example field distribution and electrostatic pressure for a bias voltage $V = -10$ V, tip radius $R = 20$ nm, tip-surface separation $d = 1$ nm, and dielectric constant inside the film $\varepsilon = 2.5$. **a**, Eqiupotential lines of $\phi = -0.01, -0.03, -0.1, -0.3, -1, -2, -4, -6, -8, -10$ V; **b**, electric field isolines of $E = 1, 2, 4, 10, 20, 40, 100, 200, 400 \times 10^6$ V m^{-1}.; and **c**, electrostatic pressure distribution at $P = 0.02, 0.02, 0.4, 1, 2, 4, 8.97, 20, 40, 100, 200$ MPa.

The isolines of the pressure arising from the field gradient are presented in Figure S1c. The maximum value of the pressure is found directly below the idealized tip; $P = 340.4$ MPa. Substantial pressures are also developed at distances on the order of 2R away from the idealized tip. For example the pressure isoline, $P = 8.97$ MPa, comes from the origin ($r = 0, z = 0$) to $R_0 \sim 47$ nm at the film upper boundary. The pressure gradient has a large normal component directed towards the axis of symmetry indicating that induced polymer melt flow would be upward.

TEMPERATURE DISTRIBUTION: 3D HEAT TRANSFER EQUATION

Spatial-temporal temperature distribution in the polymer films was obtained through the solution to a three-dimensional heat transfer equation in cylindrical coordinates with a Joule heating source.
To solve the equation, we introduce spatial coordinates r and z related to the film thickness h as $\rho = r/h$, $\zeta = z/h$, and a relative time $\tau = t \times a/h^2$, which allowed introduction of a dimensionless temperature function u: $u = (T - T_0) \times \kappa \times \sigma / (h^2 \times j^2)$. Here, T_0 is the temperature of the environment, κ and σ are thermal and electrical conductivities of the polymer film respectively, and j is the current density through a current cylinder defined by the dimensionless radius ρ_0. The heat transfer equation thus can be presented in the following form:

$$\frac{\partial u}{\partial \tau} = \Delta u + \theta\,(\rho_0 - \rho)\,,$$

where Δ is a Laplacian in cylindrical coordinates and θ is a Heaviside step-function. Direct application of integral Hankel and Laplace transforms yields a second-order ordinary differential equation with respect to ζ, which can be solved analytically. The result is the transformed function y:

$$y(\mathbf{p}, \zeta, s) = \rho_0 J_1(\mathbf{p}\,\rho_0)\,(1 - \mathbf{cosh}(kz) + \mathbf{tanh}(k)\,\mathbf{sinh}(kz))/(\mathbf{s}k^2), k = \sqrt{p^2 + s},$$

where **p** and **s** are Hankel and Laplace variables respectively, and J_1 is a first-order Bessel function. Original temperature function u can be calculated by performing an inverse Hankel and Laplace transforms of y numerically.

Figures S2 illustrates the variation of the temperature function u with respect to radial and axial coordinates calculated for a film thickness $h = 35$ nm and $\rho_0 = 2$.

The time to reach thermal steady state is given by

$$\tau = \frac{Ch^2 c_v \rho}{\kappa} \quad ,$$

where c_v is the heat capacity, ρ is the density, h is the film thickness, κ is the thermal conductivity, and C is the characteristic constant estimated from temperature equilibrium condition in the heat equation (C=100). For PMMA and PS, τ is 0.8 μsec and 1.4 μsec, respectively, indicating that thermal equilibrium would be established very rapidly.

MASS FLOW

For a cylinder, the steady flow velocity profile of a non-Newtonian incompressible liquid with non-slip boundary conditions is given by [S2]:

$$v(r) = \frac{n}{n+1}\left(\frac{|\nabla p|}{2k}\right)^{1/n} R_0^{n+1/n}\left\{1 - \left(\frac{r}{R_0}\right)^{n+1/n}\right\}$$

where R_0 is the radius of the cylinder of softened polymer, ∇p is the electrostatic pressure gradient, r is the radial coordinate and k and n are

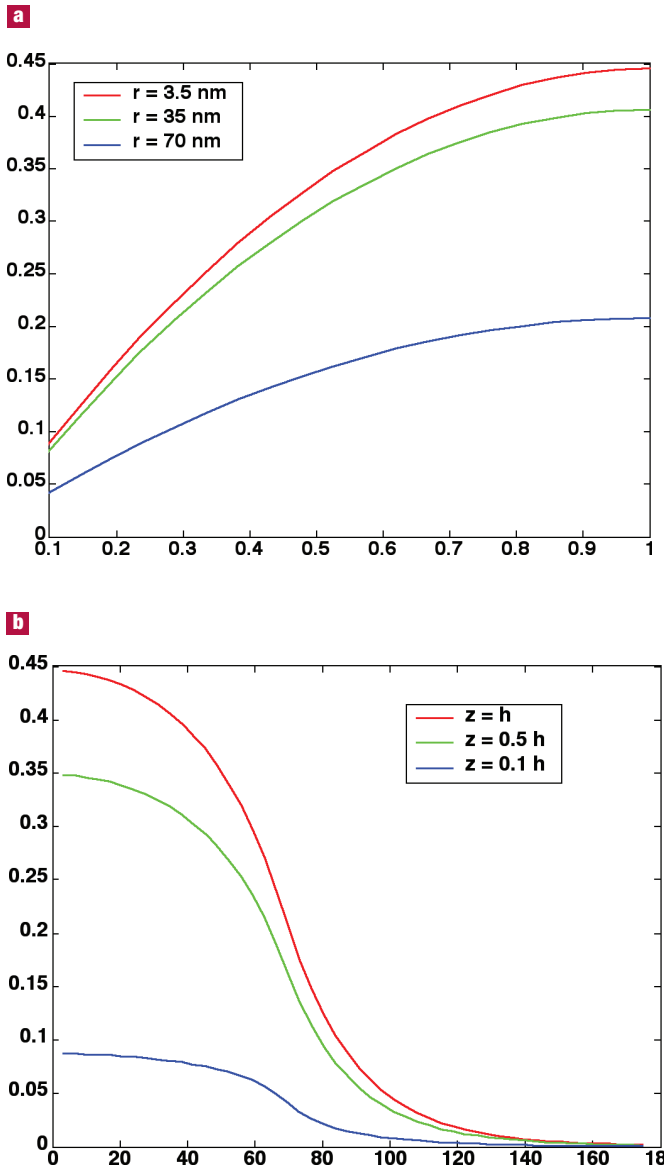

FIGURE S2

Variations of temperature with respect to radial (**a**) and axial coordinates (**b**).

material specific coefficients for a non-Newtonian liquid that obeys the power law $\tau = k\dot{\gamma}^n$ (τ is shear stress, $\dot{\gamma}$ is shear rate).

For representative values ($k = 1.6 \times 10^5$, $n = 0.4$ (for PS at 422K [S2]), $\nabla p = 2.5 \times 10^{13}$ Nm^{-3} and $R_0 = 30$ nm), Equation S3 yields $v(r) = v_0 \{ 1 - (r/R_0)^{2.9} \}$ with $v_0 = 2.35 \times 10^6$ nm/s. Thus, a 10-nm raised structure would form in 4.26 μsec, slightly longer that time to establish steady temperature distribution.

REFERENCES

S1. Lyuksyutov, S.F., Paramonov, P.B., Dolog, I.I., Ralich, R.M. Peculiarities of anomalous electronic current duting AFM-assisted nanolithography on n-type silicon. *Nanotechnology* **14**, 716–721 (2003).

S2 Tanner R.I. *Engineering Rheology* (Clarendon Press, Oxford, UK, 1985).